

# The Deep Silicate Absorption Feature in IRAS 08572+3915 and Other Infrared Galaxies

C. C. Dudley<sup>1</sup> & C. G. Wynn-Williams<sup>1,2</sup>  
Institute for Astronomy, University of Hawaii  
2680 Woodlawn Dr., Honolulu, HI 96822

## ABSTRACT

New mid-infrared (10 and 20  $\mu\text{m}$ ) spectro-photometry of the ultraluminous infrared galaxy IRAS 08572+3915 is presented. The 10  $\mu\text{m}$  spectrum reveals a deep silicate absorption feature, while the 20  $\mu\text{m}$  spectrum shows no clear evidence for an 18  $\mu\text{m}$  silicate absorption feature. An interstellar extinction curve is fitted to IRAS 08572+3915 and two other deep silicate infrared galaxies, NGC 4418 and Arp 220. It is found that pure extinction cannot explain the spectral energy distributions of these sources. On the other hand, both the strength of the silicate absorption and the overall spectral energy distributions of the three galaxies agree well with scaled-up models of galactic protostars. From this agreement, we conclude that the infrared emission comes from an optically thick dust shell surrounding a compact power source. The size of the power source is constrained to be smaller than a few parsecs. We argue that a significant portion of the total luminosities of these galaxies arises from an active galactic nucleus deeply embedded in dust.

*Subject headings:* dust — galaxies: individual: IRAS 08572+3915 — NGC 4418 — Arp 220 — galaxies: active — galaxies: nuclei — infrared: galaxies

Preprint IfA-97-31 aka astro-ph/9705242: To Appear in The Astrophysical Journal.

---

<sup>1</sup>Visiting Astronomer at the United Kingdom Infrared Telescope, which is operated by the Joint Astronomy Centre on behalf of the U.K. Particle Physics and Astronomy Research Council.

<sup>2</sup>Visiting Astronomer at the NASA Infrared Telescope Facility, which is operated by the University of Hawaii under contract to NASA.

## 1. Introduction

The nature of the power source in high-luminosity infrared galaxies is still uncertain even though the existence of these galaxies was first suggested (e.g., Kleinmann & Low 1970) more than 25 years ago. While the nature of the infrared emission from these galaxies is almost universally thought to be due to the reprocessing of shorter-wavelength radiation through absorption and reemission by dust, this averaging process leaves few clues as to the nature of the original source of shorter-wavelength radiation. Two power sources have been shown to be important through observations at many wavelengths: starbursts (Gehrz, Sramek, & Weedman 1983; Joseph & Wright 1985) and buried active galactic nuclei (AGNs) (Sanders et al. 1988). Among galaxies with luminosities in the range  $10^{11}$ – $10^{12} L_{\odot}$ , massive stars created in a burst of star formation are the main power source, but there is evidence that at luminosities above  $10^{12} L_{\odot}$ , AGNs may be an increasingly important power source (Veilleux et al. 1995; Lonsdale, Smith, & Lonsdale 1993).

Dust obscuration can hide the optical and near-infrared spectral signatures that might indicate the presence of an AGN, but dust emission provides clues that can reveal the dominant power source. By examining dust emission between 8 and 13  $\mu\text{m}$  in 60 galaxies, Roche et al. (1991) have shown that the 8–13  $\mu\text{m}$  spectra of galaxies can be classified into three types: (1) Starbursts and other galaxies with H II regionlike optical spectra show 8–13  $\mu\text{m}$  spectra dominated by a family of infrared bands commonly attributed to polycyclic aromatic hydrocarbon (PAH) molecules (Puget & Léger 1989, but see also Duley 1989; Sakata & Wada 1989; and Ellis et al. 1994 for other laboratory analogues). PAH emission thus betrays the presence of hot stars as an important power source for the overall infrared emission. (2) Quasars and Seyfert 1 galaxies often show flat featureless spectra between 8 and 13  $\mu\text{m}$ . (3) A minority of galaxies, most of which have Seyfert 2 optical spectra, show a silicate absorption feature. Thus, energetically dominant AGNs have 8–13  $\mu\text{m}$  spectra that are quite different from starbursts. Distinguishing these three types of 8–13  $\mu\text{m}$  spectra requires only moderate spectral resolution.

In this paper, we present new observations of the ultraluminous infrared galaxy IRAS 08572+3915 ( $L_{[1-1000\mu\text{m}]} = 2 \times 10^{12} L_{\odot}$ ,  $d = 233$  Mpc,  $H_0 = 75$  km s $^{-1}$ Mpc $^{-1}$ ) that show it to have an extremely deep silicate absorption feature centered near 9.7  $\mu\text{m}$ . IRAS 08572+3915 has only the third known example of a deep silicate feature among all observed galaxies with  $L_{[1-1000\mu\text{m}]} > 10^{11} L_{\odot}$ ; the others are NGC 4418 and Arp 220 (Roche et al. 1986; Smith, Aitken, & Roche 1989). It is our thesis here that the presence of a deep silicate feature in these three galaxies cannot be explained by a simple cold dust screen model, but that these three galaxies contain a power source surrounded by a optically thick shell of emitting dust with a geometry that resembles that of a scaled-up model protostar. Such a scaling (or indeed simply the notion that the dust emission is optically thick) leads to the conclusion that a major power source of deep silicate infrared galaxies is contained within a region too small to be attributed to a starburst. An energetically dominant AGN is the most likely alternative.

## 2. Observations and Data Reduction

### 2.1. Spectroscopy

IRAS 08572+3915 was observed on the nights of UT 1992 February 16 and UT 1994 February 8 at 8–13  $\mu\text{m}$ , and on the night of UT 1994 February 7 at 17–24  $\mu\text{m}$ . The cooled grating spectrometer (CGS3) (see Cohen & Davies 1995 for a description) mounted at the Cassegrain focus of the 4 m United Kingdom Infrared Telescope (UKIRT) on Mauna Kea in Hawaii was used to make the observations. The data of UT 1992 February 16 and UT 1994 February 7 were obtained under good conditions. The 8–13  $\mu\text{m}$  data of UT 1994 February 8 were of poor quality due to both variable transparency and thermal emission from cirrus clouds, and will not be discussed further except to say that they tend to confirm the data taken under good conditions, albeit at a much lower signal-to-noise ratio.

Observations at 8–13  $\mu\text{m}$  were performed using the low-resolution grating mode of CGS3 with a resolution of  $\lambda/\Delta\lambda \approx 50$  and a circular aperture with 5''.5 full width at 10% power, while observations at 17–24  $\mu\text{m}$  used the 20  $\mu\text{m}$  grating mode with  $\lambda/\Delta\lambda \approx 70$  and a smaller 3''.26 aperture to improve the signal-to-noise ratio by admitting less background emission. In both cases observations were centered on the 3.6 cm radio position published by Condon et al. (1991). The centers of the apertures were determined with respect to the optical guide camera by peaking up on infrared bright stars, and the apertures were centered on the radio position by offsetting from a nearby Carlsberg Meridian Catalog star. Pointing was maintained to  $\sim 1''$  rms by auto-guiding on a field star in the guide camera field of view.

Two interlacing grating positions were required to sample fully the spectral resolution, resulting in spectra of 64 data points spaced by 0.1  $\mu\text{m}$  for 8–13  $\mu\text{m}$  and by 0.14  $\mu\text{m}$  for 17–24  $\mu\text{m}$ . For the 8–13  $\mu\text{m}$  spectrum the observations consist of 60 beam-switched pairs of 30 s each (on source) and for the 17–24  $\mu\text{m}$  spectrum, 96 pairs of 20 s each, for each grating position. Grating shifts occurred after 10 pairs at 8–13  $\mu\text{m}$  and after 16 pairs at 17–24  $\mu\text{m}$ . Background subtraction was performed with a beam separation of 30'' for the 8–13  $\mu\text{m}$  data and 20'' for the 17–24  $\mu\text{m}$  data with the chop direction NE–SW in both cases.

For the 8–13  $\mu\text{m}$  spectrum, data shortward of 7.7  $\mu\text{m}$ , between 9.2 and 10.1  $\mu\text{m}$ , and longward of 13.2  $\mu\text{m}$  have been rejected due to poor atmospheric transmission. For the 17–24  $\mu\text{m}$  spectrum, data were rejected where the transmission was less than 30% of the maximum (atmosphere and filter) based on observations of HR 2990. Additionally, data between 10.1 and 11.8  $\mu\text{m}$  have been combined into a single bin to improve the signal-to-noise ratio.

Each spectrum was flux calibrated by dividing it by the spectrum of HR 2990 with  $N = -1.24$  and  $Q = -1.21$  (Tokunaga 1984) and by assuming a blackbody temperature of 5000 K. For the 8–13  $\mu\text{m}$  spectrum, observations of IRAS 08572+3915 were all made within 0.1 airmasses of the observation of the standard. For the 17–24  $\mu\text{m}$  spectrum two groups of observations of IRAS 08572+3915 were calibrated with two separate observations of the standard, such that the

same condition on the difference in airmass was obtained, and they were subsequently combined. No further corrections for airmass were applied. Both the object and standard spectra were calibrated in wavelength prior to division by the standard by means of higher spectral order measurements of emission lines emitted in the range 2.0–2.4  $\mu\text{m}$  by a Kr lamp as described by Hanner, Brooke, & Tokunaga (1995). We estimate the absolute flux calibration to be better than 15% for the 10  $\mu\text{m}$  spectrum and better than 30% for the 20  $\mu\text{m}$  spectrum, and the wavelength calibration to be better than half a resolution element.

## 2.2. Photometry

In order to extend wavelength coverage to shorter wavelengths, IRAS 08572+3915 was also observed on the night of UT 1997 January 6 under good conditions using NSFCAM on the NASA 3 m Infrared Telescope Facility (IRTF) on Mauna Kea, Hawaii. The camera detector was a  $256 \times 256$  pixel InSb array and the camera plate scale was set to  $0''.15$ . Three filters were used with central wavelengths at (and spectral FWHMs of) 2.21 (0.39), 3.78 (0.59), and 4.77 (0.23)  $\mu\text{m}$ . Ten pointings of 10 to 20 s each were made in each filter with a  $10''$  N-S offsets between pairs of images, and with each pair offset from the other four using a domino 5 pattern of offsets with a  $5\sqrt{2}''$  diagonal spacing. The standard star HD 22686 was also observed with five pointings for each filter in a domino 5 pattern and within 0.2 airmasses of the observations of IRAS 08572+3915. Bias subtraction was performed by subtracting alternate pointings for the galaxy, and subtracting the average of the four alternative frames for the standard. The difference images were flattened using the median normalized difference of a 1 s and a 0.5 s dome flat for the 2.21  $\mu\text{m}$  data, and by using the median of the normalized images for the 3.78 and 4.77  $\mu\text{m}$  data. Hot pixels were replaced by the median of their nominally performing neighbors in a  $3 \times 3$  pixel box. The difference images were shifted according to their centroids and summed. Flux densities for the galaxy in each filter were estimated by comparing the total number of counts within a  $4''.5$  diameter synthetic circular aperture above the average counts in a concentric annulus of inner diameter  $4''.5$  and outer diameter  $5''.4$  to the same measure of the standard star data scaled to match in integration time. The 2.21  $\mu\text{m}$  magnitude of the standard was taken to be 7.195 (Elias et al. 1982) and assumed to be 7.2 for the observations at the other two wavelengths.

## 3. Results

In Figure 1, our 8–13 and 17–24  $\mu\text{m}$  CGS3 spectra of IRAS 08572+3915 are presented along with photometric measurements at a variety of wavelengths. Given the very different spectral resolution and different passband coverage, we find good agreement between the photometric measurements and our spectra. The agreement at 12.5  $\mu\text{m}$  allows a limit on source variability to be set at less than 30% over 5 years.

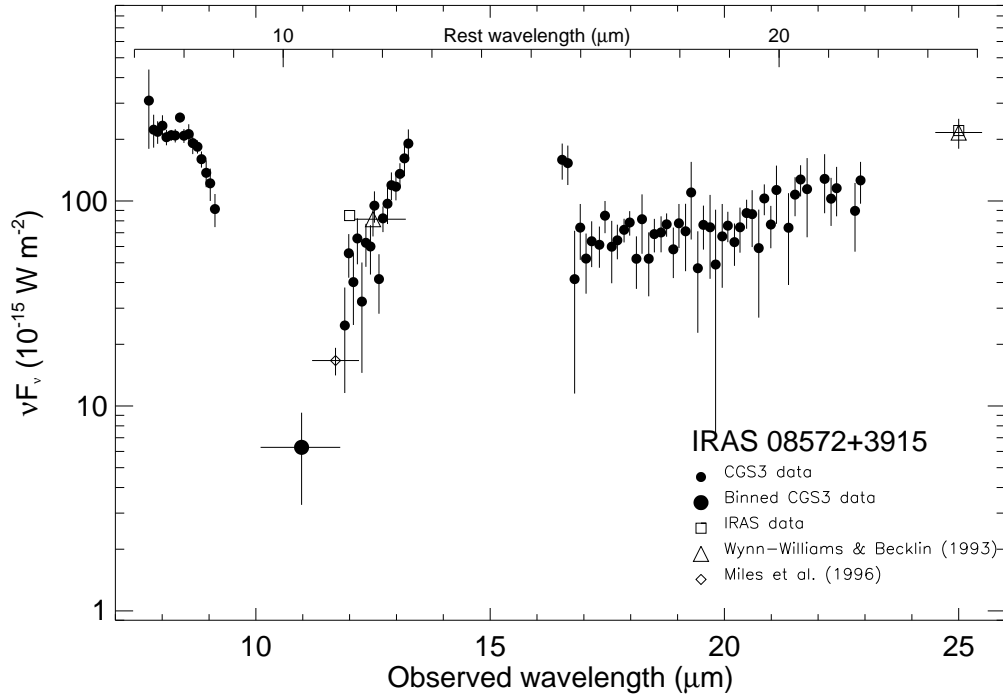


Fig. 1.— The 10 and 20  $\mu\text{m}$  CGS3 spectra of IRAS 08572+3915 are presented along with photometry from the literature. The observed wavelength is given on the upper and lower bounding box scale, and the rest wavelength ( $1 + z = 1.058$ ), based on the millimeter spectroscopy given in Sanders et al. (1989), is shown near the top of the figure. The small circles are independent spectral data points, while the large circle is data binned between 10.1 and 11.8  $\mu\text{m}$  (observed wavelength). The photometric data are from Wynn-Williams & Becklin (1993) (open triangles) and Miles et al. (1996) (open diamond) in  $5''.5$  and  $4''.6$  apertures, respectively, and IRAS data (open squares) from Soifer et al. (1989). Vertical lines on data points represent  $1\sigma$  errors, while horizontal lines indicate photometric passbands.

The data show strong silicate absorption centered near  $9.7 \mu\text{m}$  (rest wavelength), but there is no clear indication of silicate absorption centered near  $18 \mu\text{m}$  (rest wavelength) such as that seen toward the Galactic Center (McCarthy et al. 1980). No detectable evidence of the  $11.3 \mu\text{m}$  PAH emission feature ( $F(11.3\mu\text{m}) \leq 0.7 \times 10^{-15} \text{ W m}^{-2} 3\sigma$ ) is observed. Two other spectral features commonly seen in starburst galaxies, the  $8.6 \mu\text{m}$  PAH feature and the  $12.8 \mu\text{m}$  [Ne II] feature, have not been measured due to the redshift of the source imposing a coincidence with telluric  $\text{O}_3$  and  $\text{CO}_2$  bands, respectively.

Table 1 presents our new photometric data for IRAS 08572+3915 at  $2.21$ ,  $3.78$ , and  $4.77 \mu\text{m}$ . We estimate these data to be accurate to 20%. The  $3.78$  and  $4.77 \mu\text{m}$  data confirm the trend seen at shorter wavelengths that IRAS 08572+3915 displays a strong nonstellar continuum component that is dominant at wavelengths longer than  $2 \mu\text{m}$ .

The measured flux densities reported in Table 1 are somewhat higher than, although not incompatible with, those that have been previously reported. Observations using  $5''$  apertures at  $2.2 \mu\text{m}$  have been reported by Sanders et al. (1988) and Young et al. (1996) who give  $3.75$  and  $3.42 \pm 0.07 \text{ mJy}$ , respectively, for the NW source. Carico et al. (1990) and Zhou, Sanders, & Wynn-Williams (1993) report  $3.2 \pm 0.2$  and  $3.0 \pm 0.6 \text{ mJy}$  respectively using  $2''.5$  synthetic apertures. Using the SE source to perform differential photometry, we have compared our  $2.21 \mu\text{m}$  image with the  $2.15 \mu\text{m}$  image of Sanders et al. (1997), and we find our new observations to be  $\sim 25\%$  brighter than their slightly shorter wavelength observations; however this may be a result of the large H–K color of this object (Carico et al. 1990). Our  $3.78 \mu\text{m}$  flux density is also 20% higher than that reported by Sanders et al. (1988) ( $40 \text{ mJy}$ ). We interpret these results as tentative, but not conclusive, evidence for variability in IRAS 08572+3915.

#### 4. Discussion

Table 1. Near-Infrared Photometry for IRAS 08572+3915

$\lambda$ ( $\mu\text{m}$ )	$f_\nu$ (mJy)
2.21	$4.4 \pm 0.9$
3.78	$50 \pm 10$
4.77	$100 \pm 20$

#### 4.1. Infrared Galaxies with Deep Silicate Absorption

IRAS 08572+3915 is the third infrared galaxy in which a deep silicate absorption feature has been found, the others being NGC 4418 (Roche et al. 1986) and Arp 220 (Smith et al. 1989). These three sources have other features in common in addition to the similarity of their mid-infrared spectra. All show relatively warm far-infrared color temperatures and compact radio nuclei. Additionally, they have  $L_{\text{IR}}$  to  $L_{\text{CO}}$  ratios that are high compared to both infrared-emitting disk galaxies and luminous infrared galaxies taken as a class.

The three galaxies are morphologically diverse. NGC 4418 is a normal barred spiral galaxy (SAB) (de Vaucouleurs et al. 1991), and IRAS 08572+3915 has a disturbed morphology with a projected separation between optical nuclei of  $\sim 7$  kpc (Sanders et al. 1988). Arp 220 appears to be an advanced galaxy-galaxy merger with an average  $2.2 \mu\text{m}$  surface brightness profile similar to an elliptical galaxy (Wright et al. 1990), a double nucleus with a projected separation of  $\sim 360$  pc at  $2.2 \mu\text{m}$  (Graham et al. 1990), and a much obscured central region displaying a number of closely spaced hot spots at optical wavelengths (Shaya et al. 1994).

Spectra of the three galaxies at wavelengths shorter than  $8 \mu\text{m}$  exhibit a variety of phenomena. At visible wavelengths IRAS 08572+3915 and Arp 220 display the type of spectra characteristic of a low-ionization nuclear emission region (LINER) (Veilleux et al. 1995), while NGC 4418 is classified as AGN-like by Armus, Heckman, & Miley (1989), but with extremely weak emission features (Roche et al. 1986). At near-infrared wavelengths Arp 220 shows a deep  $2.3 \mu\text{m}$  CO absorption (Goldader et al. 1995). NGC 4418 shows strong  $Q$ -band  $\text{H}_2$  emission (Ridgway, Wynn-Williams, & Becklin 1994). IRAS 08572+3915 is dominated by a red continuum at  $2.2 \mu\text{m}$  (Goldader et al. 1995) and an unusually strong  $3.4 \mu\text{m}$  dust absorption feature (Wright et al. 1997), the first such observed in an external galaxy.

Spectral energy distributions for the three galaxies are plotted in Figure 2. In the case of NGC 4418 we have excluded from our plot data that appear as upper limits in the range  $9.4\text{--}11.1 \mu\text{m}$ . The spectrophotometric data for Arp 220 are corrected for contamination by a starburst component responsible for  $\sim 2\%$  of the  $8\text{--}1000 \mu\text{m}$  infrared emission by subtraction of the spectrum of NGC 7714 (Phillips, Aitken, & Roche 1984) scaled by a factor of 0.3, following Smith et al. (1989). However, we have regridded the spectrum of NGC 7714 to the sampling of the spectrum of Arp 220 rather than employing a smoothed version. We note that the subtraction of the starburst component is important only near the  $9.7 \mu\text{m}$  minimum and near  $11.3 \mu\text{m}$ ; it leaves the rest of the spectrum largely unchanged.

#### 4.2. Silicate Fitting

As a first step toward interpreting the silicate absorption features in the three galaxies, we attempted to fit their  $8\text{--}13 \mu\text{m}$  spectra by a model consisting of a power-law energy source

( $S_\nu \propto \nu^{-\alpha}$ ) behind a screen of cold dust. The extinction curve we used for the dust model,  $\tau(\lambda)$ , is that of Mathis (1990) for  $R_V \sim 3$ . It includes 9.7 and 18  $\mu\text{m}$  silicate features  $\tau_{\text{Sil}}(\lambda)$ , the shapes and relative strengths of which are taken from Draine & Lee (1984), plus a component of continuous absorption,  $\tau_{\text{Cont}}(\lambda)$ , that is proportional to  $\lambda^{-1}$  over the wavelength range of interest. Mathis lists values for his extinction curve at only a few wavelengths; we generated a much more closely sampled version of Mathis’ extinction curve between 8 and 13  $\mu\text{m}$  from the  $\mu$  Cep emissivity curve given by Roche & Aitken (1984). For the 18  $\mu\text{m}$  feature we have adopted a feature profile derived from the new *Infrared Space Observatory (ISO)* observations of the absorption seen against circumstellar carbon dust emission heated by Wolf-Rayet stars. Details are given in the Appendix. According to this extinction model, the silicate feature component contributes 3 times as much extinction at 9.7  $\mu\text{m}$  as the continuum extinction but nothing outside the range 8–25  $\mu\text{m}$  (i.e.,  $\tau_{\text{Sil}}(9.7) = 3 \times \tau_{\text{Cont}}(9.7)$ ).

Including both continuum and feature extinction allows us to estimate the total extinction ( $\tau_{\text{Tot}}(\lambda) = \tau_{\text{Cont}}(\lambda) + \tau_{\text{Sil}}(\lambda)$ ) somewhat akin to the strategy of Willner (1977), as well as  $\tau_{\text{Sil}}(9.7)$ , which is defined observationally (Aitken & Jones 1973) as

$$\tau_{\text{Sil}}(9.7) = \ln \left( \frac{F_\lambda(8) + F_\lambda(13)}{2 \times F_\lambda(9.7)} \right).$$

However, in the case of the three galaxies in question, saturation of the feature causes  $F_\lambda(9.7)$  to be poorly determined, and it was necessary to fit a silicate profile over the whole range (7.7–13.2  $\mu\text{m}$ ) to make any estimate at all. Additionally, as can be seen in Figure 1, the rest wavelength 13  $\mu\text{m}$  is not observed for IRAS 08572+3915 due to its redshift; our estimate of  $\tau_{\text{Sil}}(9.7)$  relies therefore upon an extrapolation of the fit to 13  $\mu\text{m}$ . We did not attempt to fit simultaneously the 17–24  $\mu\text{m}$  data for the three galaxies.

In fitting our extinction model, we have employed a modified version of Bevington’s (1969) nonlinear least-squares fitting routine provided with the data language IDL version 4.0. Three free parameters in combination with our interstellar extinction model have been employed. The free parameters are the power-law exponent ( $\alpha$ ), the scaling, and the amount of extinction ( $\tau_{\text{Tot}}(\lambda)$ ). The fit has been made to data in 5 to 6 bins chosen to have roughly equivalent signal-to-noise ratios. On each iteration of the fit, the model was binned in the same manner as the data before the  $\chi^2$  estimation was made. In the case of IRAS 08572+3915, data between 9.2 and 10.1  $\mu\text{m}$  have been excluded from the fit where telluric  $\text{O}_3$  absorption makes data less reliable. In the case of NGC 4418, data appearing as upper limits close to the 9.7  $\mu\text{m}$  minimum were not included in the fit, leading to a somewhat lower estimate of the silicate optical depth at 9.7  $\mu\text{m}$  than that given by Roche et al. (1986), while in the case of Arp 220, we measure a somewhat deeper silicate feature than that reported by Smith et al. (1989). We ascribe the difference to our slightly different method of subtracting the starburst component as noted in § 4.1. For both NGC 4418 and Arp 220 our estimates of  $\tau_{\text{Sil}}(9.7)$  agree with the previous estimates to within 25%.

The optical depths and power-law exponents from our best fits are indicated in Figure 2, where  $\tau_{\text{Sil}}(9.7)$ ,  $\tau_{\text{Tot}}(9.7)$ , and  $\alpha$  are as defined above.



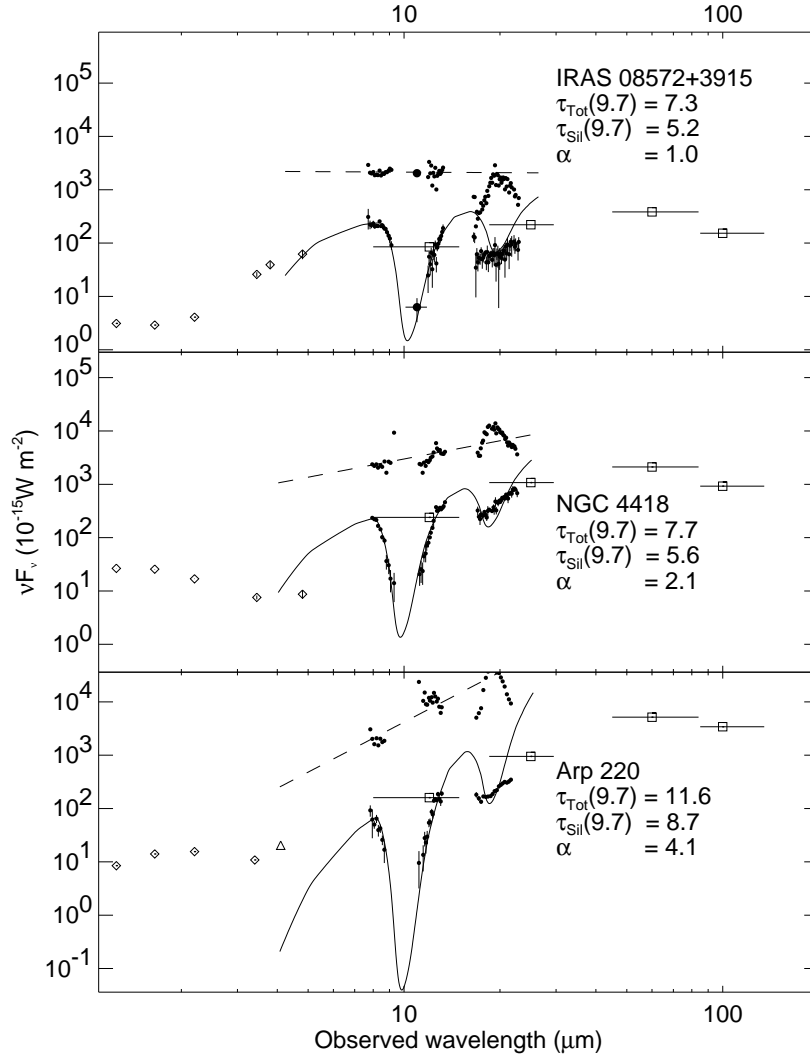


Fig. 2.— The 1.25–120  $\mu\text{m}$  spectral energy distributions of the three galaxies with deep silicate absorption features are shown. The 8–24  $\mu\text{m}$  spectroscopy (filled circles with error bars) is from this work for IRAS 08572+3915, from Roche et al. (1986) for NGC 4418, and from Smith et al. (1989) for Arp 220. The 8–13  $\mu\text{m}$  spectral data for Arp 220 have been corrected for a starburst component. For each galaxy, two series of points are plotted for the 8–24  $\mu\text{m}$  data. The lower points are the observed data, while the upper points (without error bars) represent the result of deextinguishing the data to provide the best-fit power-law spectral energy distribution over the range 8–13  $\mu\text{m}$  (see § 4.2). The dashed line is the resulting best-fit power-law model without the effects of extinction, and the solid line is the best-fit model including the effects of extinction. The broad-band photometric points (open squares) between 12 and 100  $\mu\text{m}$  are from Soifer et al. (1989). The 1.25–3.4  $\mu\text{m}$  photometry (open diamonds) for IRAS 08572+3915 and Arp 220 is taken from Zhou, Wynn-Williams, & Sanders (1993), with the addition of our new 3.8 and 4.8  $\mu\text{m}$  photometry for IRAS 08572+3915 and a 4.1  $\mu\text{m}$  continuum point for Arp 220 from DePoy, Becklin, & Geballe (1987) (open triangle). The 1.25–4.8  $\mu\text{m}$  photometric data for NGC 4418 were obtained with a 5'' aperture at UKIRT using the near-infrared photometer UKT9 on UT 1991 December 6 (Dudley 1997).

### 4.3. Problems with the Cold Screen Model for Deep Silicate Infrared Galaxies

Problems arise in attempting to explain the presence of the deep silicate feature as foreground extinction by cold dust.

First, there is no clear evidence for the predicted 18  $\mu\text{m}$  silicate absorption feature in any of the three galaxies. The difference is seen in Figure 2 and also in more detail in Figure 3, which compares the observations of the three galaxies with the expected shape and depths of the 18  $\mu\text{m}$  silicate feature predicted from the measured 9.7  $\mu\text{m}$  silicate optical depths. Roche et al. (1986) have argued that in the case of NGC 4418, the center of the 18  $\mu\text{m}$  feature may be shifted to a shorter wavelength, possibly as a result of differing dust composition, but given the larger redshift of IRAS 08572+3915, such a shorter wavelength minimum should be clearly evident in the 17–24  $\mu\text{m}$  spectrum of IRAS 08572+3915 even if centered at 17  $\mu\text{m}$ . Note that the 16–24  $\mu\text{m}$  spectrum of Arp 220, unlike that at 8–13  $\mu\text{m}$ , does not have a starburst component subtracted. The weakness of the 18  $\mu\text{m}$  silicate feature in this galaxy could be due partly to its being filled in by some starburst emission.

Second, invoking a cold foreground screen of dust to explain the appearance of the 8–13  $\mu\text{m}$  spectra of deep silicate infrared galaxies runs into serious difficulty if the background source is an extended starburst, as in most high-luminosity infrared galaxies. The typical diameter of starbursts in high-luminosity infrared galaxies is of the order of a few hundred pc (Condon et al. 1991; Wynn-Williams & Becklin 1993). To produce a silicate optical depth of 5 in such a galaxy spectrum would require a “wall” of at least this diameter with visual extinction of  $A_V \sim 75\text{--}90$  mag (Aitken 1981) and a column density of  $N_H \sim 1.5 \times 10^{23} \text{ cm}^{-2}$  if the gas to dust ratio is standard. This high value of the column density must be maintained throughout the “wall” or the silicate feature will be filled in by emission from hot dust in H II regions and photo-dissociation regions emerging through gaps in the “wall.” We would expect that such an extended high column density screen should quickly become clumped, leaving holes of lower column density. We thus believe that the presence of a deep silicate absorption feature is incompatible with an extended starburst origin for the power source in these galaxies, irrespective of the presence or absence of PAH features in their spectra.

Third, the spectral energy distributions shown in Figure 2 are incompatible with the cold absorber model if spherical symmetry is assumed for the sources. For a hot object that is completely surrounded by a cold dust shell, energy absorbed in the UV through mid-infrared must be reradiated at far-infrared wavelengths. In a  $\log \nu F_\nu$  versus  $\log \lambda$  plot, such as Figure 2, the reradiation process can be visualized as a rightward horizontal shift along the  $\log \lambda$  axis assuming that the spectral energy distributions of the of the heating source and reradiating source have approximately the same width in  $\log \lambda$ . But, as seen in Figure 2, the calculated source flux at 10  $\mu\text{m}$  matches or exceeds the maximum observed (i.e., reradiated) flux at far-infrared wavelengths in all three sources. In the case of IRAS 08572+3915 the excess is a factor of 5–6. If we are to believe that IRAS 08572+3915 contains an object with a power-law energy distribution given

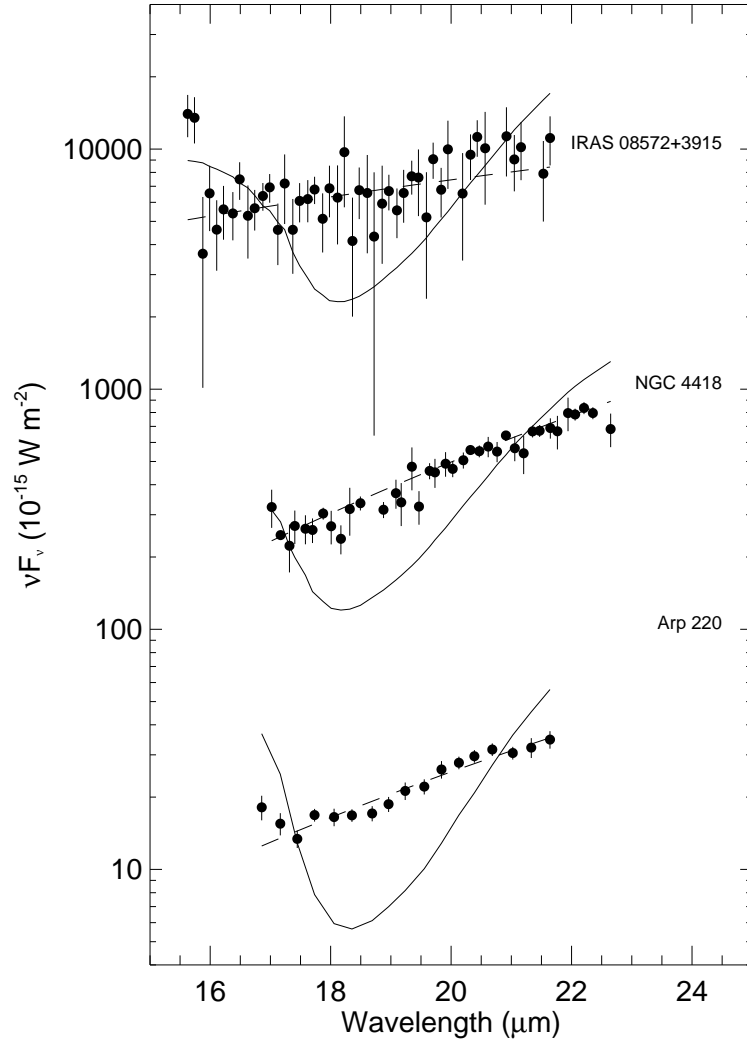


Fig. 3.— A detailed comparison of the 16–24  $\mu\text{m}$  spectra of each of the three galaxies is made with the expected shape and depth of the 18  $\mu\text{m}$  silicate feature (solid line). The sources for the spectral data are the same as in Figure 2. In each case a power-law (dashed line) gives a much better fit to the spectrum than that produced by fitting a power-law extinguished by the amount of extinction predicted from the 9.7  $\mu\text{m}$  feature. For clarity, the spectrum of IRAS 08572+3915 was shifted to its rest wavelength, and scaled up by a factor of 100, while the Arp 220 spectrum was scaled down by a factor of 10.

by the dashed line in Figure 2, then four-fifths of its power must be lost to space without being intercepted by dust. Given the large column density of dust in the line of sight to the core of IRAS 08572+3915, we consider such a geometry unlikely. Thus, this effect also calls into question the appropriateness of interpreting the deep silicate features as arising from pure extinction.

None of the above problems by itself completely eliminates the possibility that the 8–13  $\mu\text{m}$  spectra originate from cold dust, but the doubt that they raise collectively encourages us to look at other explanations for the spectra. The most promising alternative is discussed in the next section.

#### 4.4. The Protostar Analogue

The only other known infrared astronomical objects that have confirmed silicate absorption features as strong as those of the three galaxies under discussion are certain luminous “protostars” in galactic star-forming regions. Prime examples are W3 IRS5 (Aitken & Jones 1973; Willner 1977) and W33 A (Capps, Gillett, & Knacke 1978), which are thought to be new stars (protostars rather than young stellar objects, although at high mass this distinction breaks down due to rapid evolution toward the main sequence) that are still deeply embedded in the material out of which they have formed. It would be unreasonable to invoke a multitude of individual protostars to explain the present data (because other phases of star formation would dominate the mid-infrared spectrum in a composite spectrum), but we can consider the physical conditions in galactic protostars as an analogue for understanding deep silicate infrared galaxies.

In such luminous protostars the deep silicate feature is understood to arise not from pure absorption by cold dust, but from a centrally heated optically thick dust envelope that has a negative radial temperature gradient away from the power source (Scoville & Kwan 1976; Kwan & Scoville 1976). We observe a deep silicate feature because we are observing only to an optical depth of order unity at any given wavelength and we see to deeper (and therefore hotter) layers at 8 and 13  $\mu\text{m}$  than at 9.7  $\mu\text{m}$ , where the dust opacity is larger. The depth of the 9.7  $\mu\text{m}$  silicate feature is thus a result of differences in the source function at different optical depths of the dust envelope. These differences can be especially large if the emission at 10  $\mu\text{m}$  is coincident with the Wien side of the Planck function.

The problems with the cold screen model discussed in § 4.3 are accounted for naturally in the Kwan and Scoville model. The weakness of the 18  $\mu\text{m}$  silicate absorption feature can be understood because in the 20  $\mu\text{m}$  region, we are both looking deeper into the dust envelope and looking at a wavelength range that is closer to the peak of the Planck function, so that the depth of the 18  $\mu\text{m}$  feature is less than would be expected for pure extinction based on the 9.7  $\mu\text{m}$  depth. Further, only a compact source is required so that covering an extended source is no longer a difficulty. Finally, energy is conserved in the Kwan and Scoville model, so that it is no longer necessary to postulate the loss of energy to space, particularly in the case of IRAS 08572+3915.

We have examined the analogy with galactic protostar models further by comparing the three galaxies’ spectra with the grid of spherical protostar models calculated by Rowan-Robinson (1982). We have chosen these calculations over later work (Efstathiou & Rowan-Robinson 1990; Adams & Shu 1986) because they rely upon fewer geometrical assumptions but include the effect of scattering with an assumed isotropic phase function, which can make an important contribution to the emission near  $2 \mu\text{m}$ .

These calculations describe the transfer of radiation originating from a central UV thermal source through a spherically symmetric dust shell. The inner radius of the dust shell is set by the assumed dust sublimation temperature (1000 K), while the outer radius is assumed to be a multiple of the inner radius (typically 1000). The two most important parameters affecting the spectral shape of the emergent radiation examined in these models are the total optical depth at UV wavelengths and the change of density with radius; some effect is also seen as a result of varying the extent of the outer radius. Because of the high optical depth at UV wavelengths in these models, they are insensitive to the precise spectral energy distribution of the central energy source, and at radii greater than the dust sublimation radius, essentially all the radiation is dust emission. In the wavelength region  $5\text{--}24 \mu\text{m}$  the model dust opacity used by Rowan-Robinson (1982) is in essence the same as that employed in this paper in that the ratios of silicate to continuum opacity at the centers of the  $9.7 \mu\text{m}$  silicate and the  $18 \mu\text{m}$  silicate are nearly identical and the wavelength dependence of the continuum opacity has the same functional form. There is a difference in that the spectral shape of the  $9.7 \mu\text{m}$  silicate feature in the Rowan-Robinson models is assumed to be Gaussian rather than asymmetric in wavelength. It is also broader in wavelength so that the relevant comparison is not with the detailed spectral shapes of the silicate features, but rather with their depths.

In Figure 4 we compare the  $1.25\text{--}100 \mu\text{m}$  spectral energy distributions of the deep silicate infrared galaxies, as presented in Figure 2, with two of Rowan-Robinson’s models that differ in only one property, the UV optical depth ( $\tau_{UV} = \tau(\lambda < 0.1 \mu\text{m})$ ). It is clear that the overall match to the spectral energy distribution of the deep silicate infrared galaxies is quite good. We find the closest agreement between model and observation for Arp 220, indeed both the  $9.7$  and apparent  $18 \mu\text{m}$  feature depths are well matched. NGC 4418 appears bracketed by the two models, while IRAS 08572+3915 shows somewhat stronger emission at  $8 \mu\text{m}$  than the  $\tau_{UV} = 200$  model would predict. The relative weakness of the  $18 \mu\text{m}$  silicate feature compared to the  $9.7 \mu\text{m}$  silicate feature in the  $\tau_{UV} = 200$  model is in particular agreement with the IRAS 08572+3915 observations, while the agreement from  $2$  to  $5 \mu\text{m}$  is quite encouraging.

The density profiles of both models (i.e., with  $\tau_{UV} = 200$  and  $\tau_{UV} = 500$ ) are proportional to  $r^{-1}$ . We note that models with density profiles proportional to  $r^{-2}$  do not match the depths of the silicate features nor the overall spectral energy distributions of deep silicate infrared galaxies up to the maximum  $\tau_{UV}$  calculated ( $\tau_{UV} = 500$ ), while models with uniform density tend to overestimate the strength of the  $18 \mu\text{m}$  silicate feature.

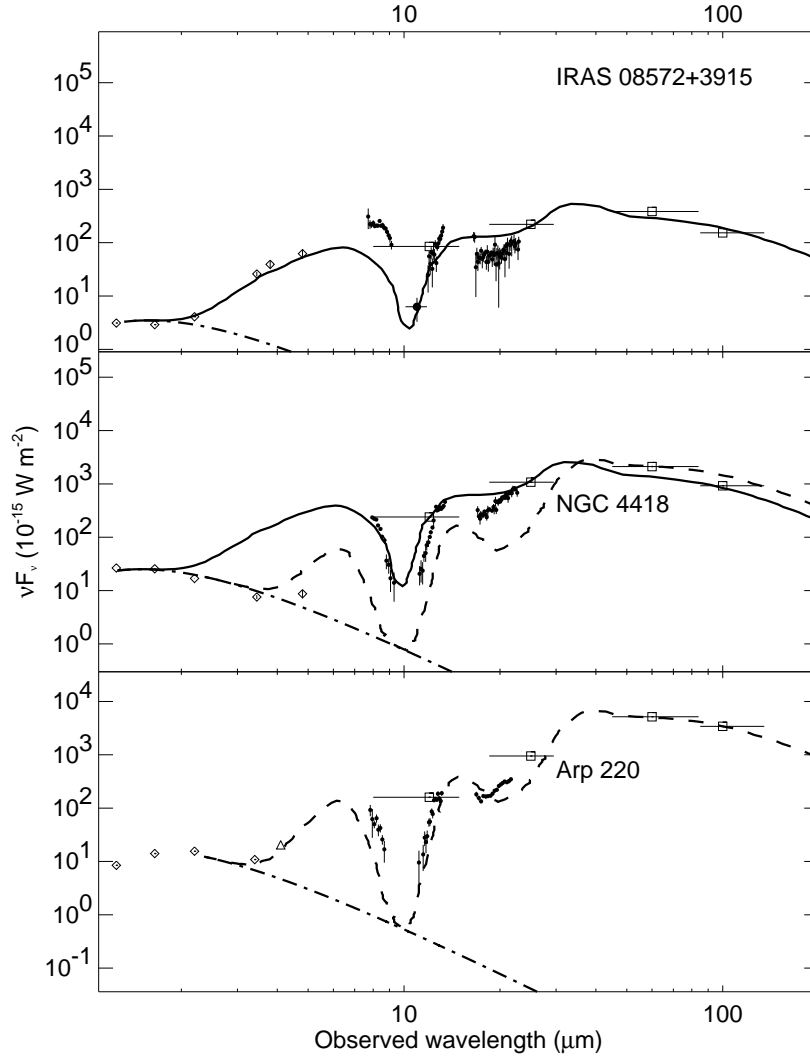


Fig. 4.— Observed spectral energy distributions of IRAS 08572+3915, NGC 4418, and Arp 220 are compared with scaled-up protostar models. The solid curves correspond to a calculation with  $\tau_{UV} = 200$ , and the dashed curves correspond to a calculation with  $\tau_{UV} = 500$ . The dot-dashed curves are 2500 K grey bodies that have been included to represent the emission from the stars in the galaxies that fall within the photometric beam.

#### 4.5. Physical Scales

The models introduced in the § 4.4 were originally calculated for galactic protostars with  $L_{\text{IR}} \sim 10^5 L_{\odot}$ , but they may be scaled (Zeljko & Elitzur 1997) to the luminosity range  $10^{11}$ – $10^{12} L_{\odot}$  by maintaining a constant emergent surface brightness and column density while the radius is increased. Thus the average density reduces as  $1/R$ , while the mass and luminosity increase as  $R^2$ , where  $R$  is a characteristic size.

Given that the detailed agreement between the models and the observations is only approximate, the following derived parameters should be taken as indicative only. The  $\tau_{UV} = 200$  model has an emergent surface brightness of  $1.4 \times 10^{-3} \text{ W m}^{-2} \text{ sr}^{-1}$  at  $25 \mu\text{m}$  at the outer radius of the model. IRAS 08572+3915 produces  $2.2 \times 10^{-13} \text{ W m}^{-2}$  at  $25 \mu\text{m}$  at a distance of 230 Mpc. Thus by scaling the model to match at  $25 \mu\text{m}$ , an angular source size of  $1.6 \times 10^{-10} \text{ sr}$  is deduced; the angular outer radius is  $1''.5$ , or 1800 pc. The inner dust sublimation radius is 1.8 pc. For an UV optical depth of 200,  $A_V=52$  so that for  $N_H = 18 \times 10^{21} A_V \text{ cm}^{-2}$  upon integration, the total gas mass for the model is  $\sim 10^{10} M_{\odot}$ .

In Table 2 we compare physical sizes, gas masses, and expected gas velocities derived from scaling the Rowan-Robinson (1982) models as shown in Figure 4 with those deduced from observations of 3.6 or 20 cm continuum and millimeter CO(1→0) emission. For reference, observed galaxy distances and infrared luminosities are given in the first two rows, while row 3 identifies the wavelength at which the scaling of the models was performed. Rows 4 and 5 give the inner radius (the dust sublimation radius) where the dust temperature is 1000 K in pc and milliarcseconds (mas), and row 6 gives the model outer radius in arcseconds. Row 7 gives the observed radio size. Row 8 gives the gas mass based on the model, while row 9 gives the gas mass based on observations of CO(1→0). Row 10 gives the expected gas line-of-sight velocity full width at half-maximum (FWHM) using the model outer radius and the model gas mass under the assumption of a virialized pressureless system with a Gaussian line profile, and row 11 gives the observed CO velocity FWHM. Row 12 gives references for the radio and CO data. Given the approximate nature of the matches between the spectral energy distributions of the galaxies and the scaled-up protostar models, we find the comparison of model and observation to be quite encouraging. A quite similar model applied to Arp 220 by Rowan-Robinson & Efstathiou (1993) leads to a very similar estimate for the inner radius. Their model has a smaller outer radius and thus has a smaller gas mass.

In addition to the physical scales that can be estimated from the model, there is another estimate of the size of the warm dust emitting region that can be made directly from the spectral data. Under the assumption that we are observing to an optical depth of order unity throughout the 8–13  $\mu\text{m}$  spectral region, we will be observing down to the same physical surface if the dust opacity is the same. In Mathis’s (1990) extinction curve, the opacities at 8 and 13  $\mu\text{m}$  are very similar, so it is possible to estimate the dust temperature at that layer. Since the emission is from an optically thick dust layer, the source size will be close to that of a blackbody of

Table 2. Scaled Protostar Models

Property	IRAS 08572+3915	NGC 4418		Arp 220
	$\tau_{UV}=200$	$\tau_{UV}=200$	$\tau_{UV}=500$	$\tau_{UV}=500$
$d$ (Mpc)	230	27		73
$L$ ( $L_{\odot}$ )	$1.3 \times 10^{12}$	$1.3 \times 10^{11}$		$1.5 \times 10^{12}$
$\lambda$ ( $\mu\text{m}$ )	25	25	60	60
$r_{\text{inner}}$ (pc)	1.7	0.44	0.46	2.1
$r_{\text{inner}}$ (mas)	1.5	3.3	3.5	5.8
$r_{\text{outer}}$ (arcsec)	1.5	3.3	3.5	5.8
$r_{\text{radio}}$ (mas)	40	200		120 <sup>a</sup>
$M_{\text{g}}$ ( $10^9 M_{\odot}$ )	10	1	2.5	25
$M_{\text{g}}(\text{CO})$ ( $10^9 M_{\odot}$ )	7	1.4		20
$2\sqrt{2 \ln 2} \times \sqrt{\frac{GM}{6R}}$ ( $\text{km s}^{-1}$ ) <sup>b</sup>	150	95	150	220
FWHM(CO) ( $\text{km s}^{-1}$ )	190	120		360
References	1, 3	2, 4		1, 4

<sup>a</sup>The radio size for Arp 220 is for the western component only.

<sup>b</sup>The virial velocity variance will be  $(GM)/(2R)$  for a system with mass  $M$  and radius  $R$  (Mihalas 1967 equation 14-14). This must be divided by a factor of 3 to give the line-of-sight variance.

References. — Radio sizes at (1) 3.6 cm from Condon et al. (1991) and (2) 20 cm Condon et al. (1990); CO data from (3) Sanders et al. (1989) and (4) Sanders, Scoville, & Soifer (1991).

Table 3. Planck Temperatures and Sizes at 8 and 13  $\mu\text{m}$

Property	IRAS 08572+3915	NGC 4418	Arp 220
$T_{8-13\mu\text{m}}$ (K)	370	280	200
$R_{8-13\mu\text{m}}$ (pc)	2	0.6	3



that temperature. In Table 3 we give the color temperatures and radii of the blackbodies that reproduce the 8 and 13  $\mu\text{m}$  flux at the distance of each source for comparison with the values derived from the models. As noted in § 4.2, our estimate of the rest wavelength 13  $\mu\text{m}$  emission for IRAS 08572+3915 is based upon an extrapolation of our fit of the interstellar extinction curve shown in Figure 2. The results of Tables 2 and 3 are consistent in that  $R_{8-13\mu\text{m}}$ , where the dust temperature is 200–400 K, is in each case larger than  $r_{\text{inner}}$  where the dust temperature is by definition 1000 K.

The most important aspect of this exercise is that it indicates that the power that is emitted predominantly at 60  $\mu\text{m}$  in deep silicate infrared galaxies conforming to this model is originally produced inside of a region with  $r_{\text{inner}}$  in the range 0.4–2 pc (Table 2). It is this feature of the model that most distinguishes it from an extended starburst model, in which the emitting dust is optically thin (at infrared wavelengths) and appears as a comparatively large solid angle region of comparatively low surface brightness.

#### 4.6. The Nature of the Power Source

In § 4.5 we argued that the spectral energy distributions of the deep silicate infrared galaxies can be fitted with a model where  $10^{11}$ – $10^{12} L_{\odot}$  is generated within a region only a few pc in size. In this section we discuss the nature of the power source.

Because of the high optical depths of dust in our suggested model, we would not expect to see any spectroscopic features associated with the sources that are produced by radiation that is highly attenuated by dust. Optical and UV lines that arise inside the dust sublimation radius would be attenuated by 50–200 mag. Since the source UV radiation is efficiently converted to  $T=1000$  K thermal emission at the dust sublimation radius, PAH emission is not expected regardless of the hardness of the source spectrum since there is little short-wavelength radiation remaining to excite emission or destroy the carriers at the radii we observe in the 8–13  $\mu\text{m}$  region. Further, we would not expect to observe variations on a timescale shorter than the light-crossing time of about a decade (see Table 3) irrespective of the intrinsic variability of the original power source.

With this much power in a small volume we are almost certain to be seeing the manifestations of an AGN of some kind, although Terlevich et al. (1993) consider that a starburst could be this compact. Most AGN models involve disklike accretion onto a black hole from a scale of  $\sim 3 \times R_S$  and larger, where  $R_S$  is the Schwarzschild radius of the black hole while short-timescale variability of known AGNs indicates sizes of order 0.05 pc. Guided by AGN models of this type, we might expect the inner regions of the source to have a disklike structure. We emphasize, however, that the dust producing the 8–13 emission from deep silicate infrared galaxies is unlikely to be very disklike itself; if the infrared radiation were coming directly from a hot disk seen partially face on, we would not see a deep silicate feature. The compact disk models of Pier & Krolik (1992) suffer

from the difficulties that (1) they present the sorts of spectral energy distributions observed in deep silicate infrared galaxies for a range of viewing angle much smaller than  $1^\circ$ , and (2) the optical spectrum should *clearly* reveal the narrow line region. The first objection might be overcome by noticing that thus far there are only three known deep silicate infrared galaxies. This argument could hold for NGC 4418 taken by itself as a member the class of luminous infrared galaxies and assuming that all luminous infrared galaxies are powered by AGNs. IRAS 08572+3915 and Arp 220 are, however, an important fraction of the bright ultraluminous infrared galaxies, and so for them compact disk models are an unlikely explanation even if all ultraluminous infrared galaxies were configured this way, without invoking the missing narrow line region argument. The tapered disk models of Efstathiou & Rowan-Robinson (1995) do not suffer as severely from restrictions on viewing angle (Efstathiou 1996), but again the optical spectra should reveal a *powerful* narrow line region, which is not the case for the known deep silicate infrared galaxies. More elaborate models such as embedded disks (along the lines of the protostar models of Adams & Shu (1986) are probably not required by the present data, but neither are they ruled out.

The model we propose here lends some support to the proposal of Sanders et al. (1988) that ultraluminous infrared galaxies are a part of an evolutionary sequence that results in optically visible quasars. If the AGNs that we suggest as the power source for the deep silicate infrared galaxies were to clear some of the enshrouding gas and dust, or alternatively, if the enshrouding gas and dust were to collapse to a disk on a timescale of  $\sim 5$  Myr, then a quasar could result. Mkn 231, which shows a Seyfert 1 optical spectrum and a silicate absorption feature (Roche, Aitken, & Whitmore 1983) that is weaker than those discussed here, might be a transitional object. Testing this possibility will require mid-infrared spectroscopic observations of a substantially larger number of ultraluminous infrared galaxies.

Sturm et al. (1996) have presented *ISO* observations of the strengths of the emission lines from Arp 220 and present two lines of evidence to suggest that this galaxy is powered by massive stars rather than by an AGN. We believe that their evidence does not conflict with the model we have suggested in this paper. Their first argument is that they see no high excitation emission lines such as would be produced by an AGN. In our model, such high excitation line emission is hidden within a very thick dust shell and would not be expected to be readily observed. Their second argument is that the line ratios of certain hydrogen and sulfur lines indicate that they come from highly reddened H II regions; when the recombination lines are dereddened, they imply Lyman continuum luminosities consistent with all the galaxy's power arising from H II regions. Our first comment is that their estimate of the extinction is based partly on a comparison of  $\text{Br}\alpha$  and  $\text{Br}\beta$  observed using a  $14'' \times 20''$  aperture with  $\text{Br}\gamma$  observed using a  $3'' \times 15''$  aperture (Goldader et al. 1995). If some of the recombination lines come from an extended region, as is suggested by the factor of 5 discrepancy between the *ISO* measurements of  $\text{Br}\alpha$  and the UKIRT observations of Depoy et al. (1987) made with a  $10''$  aperture, then some of the evidence for high extinction may be discounted. The large difference between the remaining estimates of  $A_V$ , namely, 30 mag for the  $\text{Br}\alpha$  to  $\text{Br}\beta$  ratio and the limit of  $\geq 59$  mag from the limit on the ratio of

the [S III] lines suggest that while the light from massive stars implied by these estimates of the Lyman continuum luminosity *may* be sufficient to account for the infrared luminosity of the whole galaxy, it is equally possible that it contributes only a fraction of the total luminosity.

While our model of an AGN deeply embedded in a spherical dust shell provides an attractive explanation for both the depth of the  $9.7\ \mu\text{m}$  silicate feature and the overall spectral energy distribution of the deep silicate infrared galaxies, we concede that it cannot by itself explain all the nuclear spectral features of these galaxies described in § 4.1. Also, in all three galaxies there is evidence for radio continuum emission on a scale larger than the dust sublimation radius. Some of this extended radio emission could arise from a nascent pair of jets that has not been resolved in VLA observations. It could also be due to supernova remnants from a starburst that existed before the AGN became dominant. This would be consistent with the deep  $2.3\ \mu\text{m}$  CO absorption, indicative of the presence of evolved supergiant stars, observed by Goldader et al. (1995) in the case of Arp 220. In Arp 220, the presence of two compact sources in both the radio (Norris 1988; Condon et al. 1991) and at  $12.5\ \mu\text{m}$  (Miles et al. 1996) offers the attractive possibility that the AGN and the starburst suggested by PAH emission seen in the spectrum of Smith et al. (1989) may be physically distinct. The detection of compact dust emission at  $2.7\ \text{mm}$  (Scoville et al. 1991) and mas-scale radio structure with very a high brightness temperature (Lonsdale et al. 1993) at the western source suggest that this may be the deep silicate source since, within the context of our model, such indications of phenomena differing from what is typical of spatially extended star formation might be expected. This prediction can be tested by higher spatial resolution  $8\text{--}13\ \mu\text{m}$  spectroscopic observations. The optical emission lines in the other galaxies might be produced by an as-yet undetected second nucleus, a *small* leakage of radiation from the AGN’s dust shroud, or by the effects of more penetrating X-ray radiation that are not included in our model.

## 5. Conclusions

We have presented new mid-infrared spectroscopy of the ultraluminous infrared galaxy IRAS 08572+3915 and have found the  $8\text{--}13\ \mu\text{m}$  spectrum to be dominated by a very strong silicate absorption feature. The  $17\text{--}24\ \mu\text{m}$  spectrum does not show any clear indication of the predicted  $18\ \mu\text{m}$  silicate feature. IRAS 08572+3915 is found to be a member of a group of deep  $9.7\ \mu\text{m}$  silicate infrared galaxies that include NGC 4418 and Arp 220.

We have presented fits of an arbitrary power law extinguished by interstellar extinction for all three galaxies and have shown that the calculated source flux in the  $8\text{--}13\ \mu\text{m}$  region is too high if cold shell absorption in the  $8\text{--}13\ \mu\text{m}$  region produces the far-infrared emission. This difficulty, in combination with the arguments that an extended cold screen is unworkable and that there is little evidence for the  $18\ \mu\text{m}$  silicate feature in absorption in any of the sources, leads us to try to fit a model along the lines of protostar models as a simpler and qualitatively better explanation of the data.

We have used two protostar models that differ only in optical depth to characterize the sources and make comparisons with observation at other wavelengths. We find that the observed gas mass and velocity dispersions are fairly consistent with model predictions.

Both the scaling of published protostar models and the assumption that the optical depth at 8 and 13  $\mu\text{m}$  is of order unity lead to sizes for the warm dust emission region that are smaller than a few pc.

We have argued that if the sizes derived either from the protostar models or by means of the blackbody assumption are correct, then it is very unlikely that deep silicate infrared galaxies are powered by star formation.

On the basis of these arguments, we propose tentatively that for the three galaxies considered here, a substantial portion of their infrared emission can be ascribed to AGNs nearly completely surrounded by optically thick dust shells with hot dust near the center and negative radial dust temperature gradients.

We would like to thank the UKIRT staff (Joel Aycock, Dolores Walther, and Thor Wold) for assistance at the telescope, and Tom Geballe and Gillian Wright for fruitful discussions and sharing spectral data in advance of publication. We also thank Bill Golisch, who ran the IRTF during our observations. This work has benefited from discussion with and/or sharing of work in progress by many members of the Institute for Astronomy. A few are Dave Sanders, Bob Joseph, Klaus Hoddap, Josh Barnes, George Herbig, John Hibbard, Alan Tokunaga, Ken Chambers, Jeff Goldader, Joe Jensen, and Jason Surace; we thank these and others. We thank John Dudley for a critical reading of an early draft of this paper. This work has been partially supported by NSF grant ASTR-8919563 and NASA grant NAGW-3938. The NASA/IPAC Extragalactic Database (NED) has been a constant aid. It is run by the Jet Propulsion Laboratory, California Institute of Technology, under contract with NASA. This work has also made use of NASA's Astrophysics Data System Abstract Service.

### A. The Spectral Shape of the 18 $\mu\text{m}$ Silicate Feature

The shape of the interstellar 18  $\mu\text{m}$  silicate feature is poorly determined due to its relatively lower peak absorption and greater breadth relative to the 9.7  $\mu\text{m}$  feature. The advent of *ISO* has made it possible to determine the shape of the profile with much greater precision than before. In this Appendix we derive the profile of the 18  $\mu\text{m}$  silicate feature from *ISO* Short Wavelength Spectrograph 3–30  $\mu\text{m}$  spectra of Wolf-Rayet stars published by van der Hucht et al. (1996). The advantage of using these stars' spectra as templates for the 18  $\mu\text{m}$  silicate absorption feature is that the underlying energy distribution of the star in the 3–30  $\mu\text{m}$  range arises from hot carbon dust and is therefore smooth and free of any intrinsic silicate emission features.

To derive the shape of the 18  $\mu\text{m}$  feature, we have modeled the carbon dust emission against which it is observed as originating in shells of dust at a range of temperatures following Williams, van der Hucht, & Thé (1987) in a simplified manner. The carbon dust emission from three Wolf-Rayet stars, WR 98a, WR 112, and WR 118, was modeled as arising from dust with emissivity proportional to  $\lambda^{-1}$  in 10 shells with  $T$  ranging from 350 to 1500 K in equal intervals. WR 48a and WR 104, whose spectra were also reported by van der Hucht et al. (1996), have not been modeled in the first instance because our model is too simple to give an adequate fit, and in the second instance, because the extinction is too low to make a useful estimate of the shape of the 18  $\mu\text{m}$  silicate feature. The contribution of each shell at 35  $\mu\text{m}$  was proportional to a power of the shell temperature. The interstellar extinction outside of the 18  $\mu\text{m}$  silicate feature toward the hot carbon dust was taken to have the wavelength dependence employed throughout this paper, namely, the curve given by Mathis (1990) supplemented by the 8–13  $\mu$  Cep emissivity curve given by Roche & Aitken (1984). The amount of extinction for each of the stars, WR 98a, WR 112, and WR 118, was estimated by fitting the 9.7  $\mu\text{m}$  silicate feature giving  $\tau_{\text{Sil}(9.7)}$  of 0.68, 0.63, and 0.62, respectively. Bevington’s (1969) CURVFIT program was employed to estimate the continuum flux density and the exponent of the dust shell temperature required to give the best fit to the observations in the wavelength ranges 4.5–5.8, 6.4–13.2, and 25.0–29.0  $\mu\text{m}$ . Using these parameters, the carbon dust continuum emission was estimated over the whole range 3–30  $\mu\text{m}$  for each star. We then used this derived carbon dust emission to estimate the extinction in the 18–25  $\mu\text{m}$  range. The derived extinction curves of WR 98a and WR 112 were adjusted to match WR 118 at 9.7  $\mu\text{m}$ , and the average extinction as a function of wavelength was computed from these three estimates.

Figure 5 presents the average results of our model fits. The vertical scale is silicate feature optical depth after removal of the continuous extinction component, and the horizontal scale is wavelength. Our derived 18  $\mu\text{m}$  silicate profile is given by the thin line in Figure 5. The thick lines are the smooth estimates of the silicate features that we adopt. The one peaking at 9.7  $\mu\text{m}$  is our adopted  $\mu$  Cep emissivity curve from Roche & Aitken (1984), and the one centered at 18  $\mu\text{m}$  is our new estimate of the shape of the 18  $\mu\text{m}$  silicate feature.

We have also plotted the extinction values tabulated by Mathis (1990) less the continuous extinction and scaled to the appropriate optical depth. The differences seen between our adopted curve and Mathis’s curve (filled circles) near the peak of the 9.7  $\mu\text{m}$  feature are due to Mathis’s reliance on the quasi-empirical curve of Draine & Lee (1984), which attempts to model the silicate emission observed in the Trapezium region of the Orion Nebula. We find that the interstellar 18  $\mu\text{m}$  silicate feature may also be more peaked than that employed by Mathis (1990). We do not have the data to estimate how much the ratios of the strengths of the silicate features vary with respect to each other or how the feature strengths vary with respect to the continuous extinction on different lines of sight.

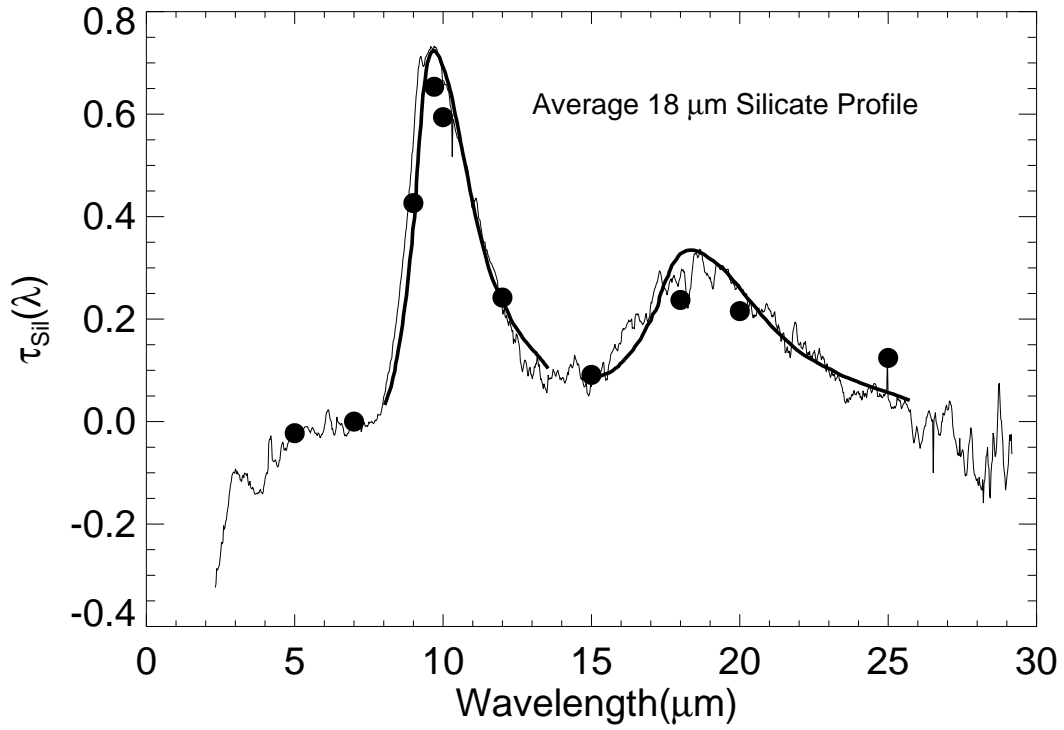


Fig. 5.— The average 18  $\mu\text{m}$  silicate feature optical depth along the lines of sight toward three Wolf-Rayet stars is presented. The thin line gives our derived estimate of the 18 silicate feature optical depth as a function of wavelength. Our adopted silicate feature profiles are shown as thick lines. The filled circles show the curve given by Mathis (1990) after subtraction of the continuous extinction.

## REFERENCES

- Adams, F. C., & Shu, F. H. 1986, *ApJ*, 308, 836
- Aitken, D. K. 1981, in *IAU Symposium 96, Infrared Astronomy*, ed. C. G. Wynn-Williams & D. P. Cruikshank (Dordrecht: Reidel), 207
- Aitken, D. K., & Jones, B. 1973, *ApJ*, 184, 127
- Armus, L., Heckman, T. M., & Miley, G. K. 1989, *ApJ*, 347, 727
- Bevington, P. R. 1969, *Data Reduction and Error Analysis for the Physical Sciences* (New York: McGraw-Hill)
- Capps, R. W., Gillett, F. C., & Knacke, R. F. 1978, *ApJ*, 226, 863
- Carico, D. P., Graham, J. R., Matthews, K., Wilson, T. D., Soifer, B. T., Neugebauer, G., & Sanders, D. B. 1990, *ApJ*, 349, L39
- Cohen, M., & Davies, J. K. 1995, *MNRAS*, 276, 715
- Condon, J. J., Helou, G., Sanders, D. B., & Soifer, B. T. 1990, *ApJS*, 73, 359
- Condon, J. J., Huang, Z.-P., Yin, Q. F., & Thuan, T. X. 1991, *ApJ*, 378, 65
- DePoy, D. L., Becklin, E. E., & Geballe, T. R. 1987, *ApJ*, 316, L63
- de Vaucouleurs, G., de Vaucouleurs, A., Corwin, Jr., H. G., Buta, R. J., Paturel, G., & Fouqué, P. 1991, *Third Reference Catalogue of Bright Galaxies*, (New York: Springer Verlag)
- Draine, B. T., & Lee, H. M. 1984, *ApJ*, 285, 89
- Dudley, C. C. 1997, Ph.D. thesis, University of Hawaii
- Duley, W. W. 1989, in *IAU Symposium 135, Interstellar Dust*, ed. L. J. Allamandola & A. G. G. M. Tielens (Dordrecht: Kluwer), 141
- Efstathiou, A. 1996, private communication
- Efstathiou, A., & Rowan-Robinson, M. 1990, *MNRAS*, 245, 275
- Efstathiou, A., & Rowan-Robinson, M. 1995, *MNRAS*, 273, 649
- Elias, J. H., Frogel, J. A., Matthews, K., & Neugebauer, G. 1982, *AJ*, 87, 1029
- Ellis, K., Guillois, O., Nenner, I., Papoular, R., & Reynard, C. 1994, in *Molecules and Grains in Space*, ed. I. Nenner (New York: AIP), 811
- Gehrz, R. D., Sramek, R. A., & Weedman, D. W. 1983, *ApJ*, 267, 551
- Goldader, J. D., Joseph, R. D., Doyon, R., & Sanders, D. B. 1995, *ApJ*, 444, 97
- Graham, J. R., Carico, D. P., Matthews, K., Neugebauer, G., Soifer, B. T., & Wilson, T. D. 1990, *ApJ*, 354, L5
- Hanner, M. S., Brooke, T. Y., & Tokunaga, A. T. 1995, *ApJ*, 438, 250
- Joseph, R. D., & Wright, G. S. 1985, *MNRAS*, 214, 87

- Kleinmann, D. E., & Low, F. J. 1970, *ApJ*, 159, L165
- Kwan, J., & Scoville, N. 1976, *ApJ*, 209, 102
- Lonsdale, C. J., Smith, H. E., & Lonsdale, C. J. 1993, *ApJ*, 405, L9
- Mathis, J. S. 1990, *ARA&A*, 28, 37
- McCarthy, J. F., Forrest, W. J., Briotta, D. A., & Houck, J. R. 1980, *ApJ*, 242, 965
- Mihalas, D. 1967, *Galactic Astronomy* (San Francisco: W. H. Freeman)
- Miles, J. W., Houck, T. L., Hayward, T. L., & Ashby, M. L. N. 1996, *ApJ*, 465, 191
- Norris, R. P. 1988, *MNRAS*, 230, 345
- Phillips, M. M., Aitken, D. K., & Roche, P. F. 1984, *MNRAS*, 207, 25
- Pier, E. A., & Krolik, J. H. 1992, *ApJ*, 401, 99
- Puget L. J., & Léger, A. 1989, *ARA&A*, 27, 161
- Ridgway, S. E., Wynn-Williams, C. G., & Becklin, E. E. 1994, *ApJ*, 428, 609
- Roche, P. F., & Aitken, D. K. 1984, *MNRAS*, 208, 481
- Roche, P. F., Aitken, D. K., Smith, C. H., & James, S. D. 1986, *MNRAS*, 218, 19P
- Roche, P. F., Aitken, D. K., Smith, C. H., & Ward, M. J. 1991, *MNRAS*, 248, 606
- Roche, P. F., Aitken, D. K., & Whitmore, B. 1983, *MNRAS*, 205, 21P
- Rowan-Robinson, M. 1982, *MNRAS*, 201, 289
- Rowan-Robinson, M., & Efstathiou, A. 1993, *MNRAS*, 263, 675
- Sakata, A., & Wada, S. 1989, in *IAU Symposium 135, Interstellar Dust*, ed. L. J. Allamandola & A. G. G. M. Tielens (Dordrecht: Kluwer), 191
- Sanders et al. 1997, in preparation
- Sanders, D. B., Scoville, N. Z., & Soifer, B. T. 1991, *ApJ*, 370, 158
- Sanders, D. B., Scoville, N. Z., Zensus, A., Soifer, B. T., Wilson, T. L., Zylka, R., & Steppe, H. 1989, *A&A*, 213, L5
- Sanders, D. B., Soifer, B. T., Elias, J. H., Madore, B. F., Matthews, K., Neugebauer, G., & Scoville, N. Z. 1988, *ApJ*, 325, 74
- Scoville, N. Z., & Kwan, J. 1976, *ApJ*, 206, 718
- Scoville, N. Z., Sargent, A. I., Sanders, D. B., & Soifer, B. T. 1991, *ApJ*, 366, L5
- Shaya, E. J., Dowling, D. M., Currie, D. G., Faber, S. M., & Groth, E. J. 1994, *AJ*, 107, 1675
- Smith, C. H., Aitken, D. K., & Roche, P. F. 1989, *MNRAS*, 241, 425
- Soifer, B. T., Boehmer, G., Neugebauer, G., & Sanders, D. B. 1989, *AJ*, 98, 766
- Sturm, E., et al. 1996, *A&A*, 315, 133



- Terlevich, R. J., Tenorio-Tagle, G., Franco, J., Rozyczka, M., & Boyle, B. J. 1993, *Rev. Mex. Astron. & Astrophys.*, 27, 59
- Tokunaga, A. T. 1984, *AJ*, 89, 172
- van der Hucht, K. A., et al. 1996, *A&A*, 315,193
- Veilleux, S., Kim, D.-C., Sanders, D. B., Mazzerella, J. M., & Soifer, B. T. 1995, *ApJS*, 98, 171
- Williams, P. M., van der Hucht, K. A., & Thé, P. S. 1987, *A&A*, 182, 91
- Willner S. P. 1977, *ApJ*, 214, 706
- Wright, G. S., James, P. A., Joseph, R. D., & McLean, I. S. 1990, *Nature*, 344, 417
- Wright, G. S., et al. 1997, in preparation
- Wynn-Williams, C. G., & Becklin, E. E. 1993, *ApJ*, 412, 535
- Young, S., Hough, J. H., Efstathiou, A., Wills, B. J., Bailey, J. A., Ward, M. J., & Axon, D. J. 1996, *MNRAS*, 281, 1206
- Zeljko, I., & Elitzur, M. 1997, *MNRAS*, in press (astro-ph/9612164)
- Zhou, S., Wynn-Williams, C. G., & Sanders, D. B. 1993, *ApJ*, 409, 149